Millimeter emission from protoplanetary disks : dust, cold gas, and relativistic electrons

Salter, D.M.

Chapter 1

Introduction

In the 1700s, after noting how the planets appeared to orbit the Sun in one direction and in roughly the same plane, several European philosophers independently postulated that our Solar System must have formed from a flattened rotating disk (see Swedenborg 1734; Kant 1755; Laplace 1796). Two centuries later, particularly in the 1960s and 1970s, theoretical models linking the collapse of interstellar molecular clouds to star birth indicated that circumstellar disks, containing the raw materials for planetary systems, are both a natural and necessary consequence of the star formation process (e.g. Bok 1948; Hayashi 1961; Larson 1969; Shu 1977). With the development of infrared detectors in the 1980s, the first observational evidence for warm circumstellar material was discovered around several main-sequence stars (e.g. Aumann et al. 1984; Smith & Terrile 1984; Strom et al. 1989; Beckwith et al. 1990). However, only by the early 1990s had advances in millimeter interferometry provided definitive proof for the existence of protoplanetary disks around young forming stars, both in the form of resolved Solar System sized dusty disks (e.g. Simon & Guilloteau 1992; Koerner et al. 1993), as well as large gaseous disks exhibiting rotating Keplerian velocity structures (e.g. Sargent & Beckwith 1987; Weintraub et al. 1989; Dutrey et al. 1993; Kawabe et al. 1993). The ground-based millimeter measurements complemented space-based optical images taken by the then newly launched Hubble Space Telescope (HST), which revealed in silhouette several protoplanetary disks (or "proplyds") in the Orion star-forming region (see Figure 1.2, and O'dell et al. 1993); and just as the ubiquity of protoplanetary disks around young stars was established, the first indirect detections of planets orbiting around other main-sequence stars followed in 1995 (see Mayor & Queloz 1995; Marcy & Butler 1996; Butler & Marcy 1996). In the 15 years since then, hundreds of both confirmed and candidate planetary systems have been identified from radial-velocity measurements (e.g. Baranne et al. 1996; Queloz et al. 2000; Santos et al. 2001; Udry & Santos 2007), photometric transits (e.g. Charbonneau et al. 2000; Henry et al. 2000; Borucki et al. 2007; Barge et al. 2008; Léger et al. 2009), gravitational microlensing (e.g. Udalski et al. 1992, 2002; Bouchy et al. 2004), and most recently by direct imaging (e.g. Marois et al. 2008; Kalas et al. 2008; Lagrange et al. 2010). Most of these extra-solar planets (or "exoplanets") differ greatly from the planets in our own Solar System, and even defy traditional theories on planet formation. Now many of the fundamental questions in modern astronomy—and in this thesis—surround a desire to identify the specific physical and chemical processes that transform circumstellar disks into the variety of planetary systems that we observe today; including, why some disks apparently fail to produce planets at all.

1.1 Origins

Star and disk formation are intricately entwined, as is their evolution. Circumstellar disks are an essential outcome of stellar birth and the central star is responsible for many important drivers of the disk evolution. Accordingly, to place the subject of disk evolution and the formation of planetary systems into its proper context, it is necessary to first review the current theory for the formation of a low-mass ($\leq 2\,M_{\odot}$) Sun-like star.

1.1.1 The Formation of Sun-like Stars

For much of human history, stars were thought to be permanent fixtures in the night sky; but rather they, too, experience a life cycle of birth, ageing, and death. The earliest stages of star formation occur hidden from sight, deep within a cold and dark molecular cloud. These clouds are distributed throughout the galaxy and were first described as "holes in the heavens" by the British astronomer Sir Frederick William Herschel (see Herschel 1785). Once believed to be empty regions absent of light, they are now recognized as some of the densest concentrations of cold dust and molecular gas (see Bergin & Tafalla 2007, for a recent reveiw), which aptly block the optical light from the stars behind them (see Figure 1.1). These same dense conditions that shield our view into the cloud, are also critical to the success of star formation itself. To form a star, a large reservoir of dust and gas is needed. Molecular clouds spanning many parsecs possess the required ingredients, as well as an inhomogenous structure that, under the influence of gravity, becomes concentrated into separate, more massive, clumps of the order one parsec in diameter. Each clump is initially supported against further gravitational collapse by thermal gas pressure, magnetic pressure, and rotational pressure, in addition to turbulence. The balance begins to shift, however, when densities in the clumps start approaching 10^3–10^4 particles per cm^{-3}, or about a factor 100–1000 times denser than the surrounding interstellar medium, sometimes with the aid of shock fronts from nearby dying stars, or supernovae.

A denser concentration of material curtails the cloud-supporting mechanisms. Higher clump densities contribute to more effective shielding of the most embedded regions from external radiation sources and the corresponding heating effects; thereby reducing the internal gas pressure. Small micron-sized dust grains, in particular, form a protective layer against the interstellar UV field, which is otherwise an effective destroyer of all but the largest, or most strongly bound, molecular compounds. The surviving molecules, in turn, provide an effective pathway to radiate energy away from the clump. Unlike atomic matter, molecules can store (angular kinetic) energy through rotation about a molecular axis. When this energy is released via transitions to lower-energy rotational states, the emitted radiation is characterized by millimeter wavelengths that more easily escape the dense region; a property that will prove invaluable for the study of disks as well. Thus, as heat is generated by the slow condensation of the clump, this energy is quickly absorbed by the molecules during collisions, and then continuously radiated away via downward rotational transitions; thereby reducing further the thermal pressure, also from new internal heat sources. Other energy input sources, like cosmic ray heating, are not enough to compensate for an energy balance now skewed toward a net energy loss. The temperature throughout the clump drops to as low as 10 K ($-263.15\,^{\circ}$C). Neutral particles now drift freely past the magnetic field lines in a process called ambipolar diffusion, while simultaneously—and in a role reversal—collisionally corraling the ions along with them into a denser centralized core. Since the ions are tied to the magnetic field, the field lines become frozen to the large-scale movements of an impending collapse; thereby limiting any potential for magnetic braking. The gravitational attraction only intensifies as the clump becomes more centrally condensed while achieving characteristic densities of $\geq 10^5$ particles per cm^{-3}. Eventually, this concentration of material reaches a critical density, sometimes expressed as the Jeans mass, and runaway gravitational collapse ensues. This is time zero ($t = 0$) for star formation. From this point forward, the

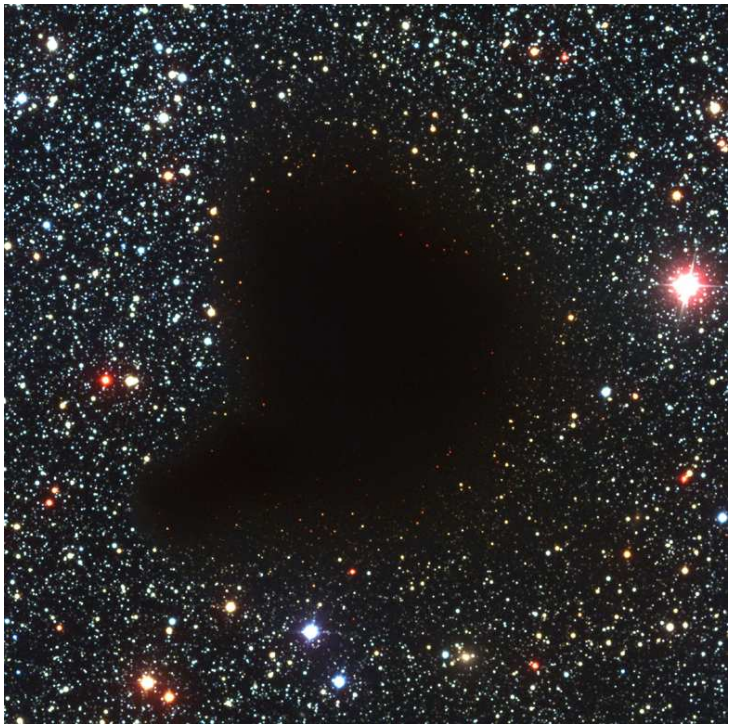

Figure 1.1 — A dark molecular cloud. An optical image of Barnard 68, a potential star formation site, as observed with the 8.2-meter VLT Antu at the Paranal Observatory in Chile. At a distance of 500 light-years from Earth, the cloud measures $\sim$0.5 light-years across. This image covers a $6.8' \times 6.8'$ region on the sky. (*Credit: ESO*)

central object will receive many names to describe its different evolutionary stages, but it may always be referred to as a young stellar object (YSO) while it is still forming.

The Four Classes of Young Stellar Objects

The dense structure is now a roughly spherical, gravitationally bound, isothermal cloud core of about 10,000 AU in size. This represents the Lada Class 0 deeply embedded phase of star formation (Lada & Wilking 1984; André et al. 1993). All of the necesary ingredients to form a star and a planetary system are presumed present (Krumholz et al. 2005), and this process that begins as an inside-out self-similar collapse of the core is expected to take 10^7 years or more to completely form a low-mass, main-sequence star similar to the Sun (Shu 1977).

In the beginning though, only a starless core exists. As material collapses in on itself from ever larger radii, the core begins to rotate in order to conserve angular momentum (Goodman et al. 1993), and the infalling envelope material slowly flattens along the direction of the rotation axis (Terebey et al. 1984; Basu 1998). Eventually a protostar forms at the center of the core, initially converting gravitational potential energy into accretion luminosity in what is sometimes known as the Kelvin-Helmholtz mechanism. Only recently have observational studies been able to reveal with some certainty the velocity field of a collapsing core, while looking to document the early conversion from an infall- to a rotationally-dominated structure (e.g. Hogerheijde 2001; Brinch et al. 2008, 2009). This velocity field transformation occurs when the initially inward free-falling material starts to collect in an accretion disk around the protostar, just outside the centrifugal radius where the rotational pressure dominates over gravity (see Cassen & Moosman 1981; Terebey et al. 1984; Yorke et al. 1993; Visser et al. 2009; Visser & Dullemond 2010). This radius moves outward over time as the disk grows and the protostar rotates faster.

The earliest evidence for a very deeply embedded Keplerian disk has now been detected in the Class I stage of the protostar development (e.g. Keene & Masson 1990; Sargent & Beckwith 1991; Chandler et al. 1994; Lommen et al. 2008; Jørgensen et al. 2009). In this second stage, the embedded source can be studied at shorter mid- to far-infrared (or micron) wavelengths due to warmed dust in the innermost regions close to the protostar. In addition, strong bipolar jets and outflows emerge to help relieve the build-up of angular momentum, and to aid the protostar in keeping a rotation rate below break-up speeds as material continues to accrete onto it. Within a period of about 10^4–10^5 years, the star begins converting deuterium for energy in its interior (Stahler 1983), strong pre-stellar winds disperse the thick envelope, the jets weaken as accretion slows, the outflow angles broaden over time, and the circumstellar disk flattens. When the central pre-main-sequence (PMS) star becomes optically visible, the low-mass source is called a classical T Tauri star (CTTS) and occupies Class II of the Lada evolutionary scheme. If a remnant envelope remains, the excess thermal emission originates primarily from the optically thick circumstellar disk ($M_{\rm disk} > M_{\rm env}$). This is the stage when we search for clues to planet formation; and thus, the main focus of the work presented in this thesis. Near the end of this stage, the PMS star may otherwise be known as a weak-line T Tauri star (WTTS) when it stops accreting material (Walter 1987). By the final Class III stage, the confirmed WTTS star is accompanied by a remnant disk, debris disk, planetary system, or nothing at all.

The final stages of star formation involve igniting nuclear fusion of hydrogen into helium within the stellar core, and then achieving hydrostatic equilibrium (or the balance between radiative pressure and gravitational contraction). When these two conditions have been satisfied, the central object has reached the zero-age main-sequence (Hayashi et al. 1962; Larson 2003). The star formation process is complete and a star is born. While the theory summarized here highlights singular low-mass star formation, we note that multiple-star systems also occur in large fractions, up to 65% of the stellar population in the middle of the main-sequence (Duquennoy & Mayor 1991), and may result from irregular fragmentation of the original cloud core (Dobbs et al. 2005; Krumholz et al. 2010). In addition, about 20% of all known exoplanets have been found in binary systems possessing stellar separations < 100 AU (Raghavan et al. 2006; Duchêne 2010). Since three of the studies presented in this thesis concern binary sources specifically, we will return periodically to their properties as well, including the challenges their stellar dynamics present to disk evolution. Finally, we remark how observations highlighting disk parameters around similarly aged PMS stars in the same cluster show significant variation (Muzerolle et al. 2000; Sicilia-Aguilar et al. 2006; Kessler-Silacci et al. 2006; Furlan et al. 2006), suggesting that the initial disk conditions resulting from this star formation process are neither consistent nor uniform (Alexander 2008), or that disk processing mechanisms vary significantly from disk to disk, or both.

In conclusion, the formation history of the star, its multiplicity, composition, mass, disk-dispersing winds, radiation field, and many other attributes, as discussed here, will all certainly impact the early circumstellar disk conditions and presumably the outcome of its evolution. However, for the purpose of the research presented in this thesis, we will focus our studies primarily on the current star and disk observables, and assume similar initial or environmental conditions to identify trends and draw conclusions about the *ongoing* disk processing, and what it means for future planets.

1.1.2 The Birth Sites of Planetary Systems

While circumstellar disks are an intrinsic consequence of the star formation process, planets are not necessarily. So when is a circumstellar disk also a protoplanetary disk? The latter term referring more specifically to a pre-cursor site for planet formation. The answers are still unclear, but ultimately, it is the direct competition between the disk dispersal timescales and the planet formation timescales that will determine the success rate for planetary systems. In this section, we discuss the general properties, trends, and major processes observed during the evolution of a circumstellar disk, with particular emphasis on

Figure 1.2 — Four protoplanetary disks in the Orion Nebula, shown in silhouette. At center, the largest disk is ∼800 AU in diameter. This image was taken in 1993 with the Wide Field and Planetary Camera 2 on board the Hubble Space Telescope, and measures 0.14 light-years across. (*Credit: C.R. O'Dell of Rice University / NASA*)

the disk dispersal mechanisms, planet formation theories, and the consequences both have for planets.

By far, the most stringent constraint on planet formation is the disk lifetime, and yet the relative impact of the main dissipation mechanisms is still not well understood. The primary dispersal mechanisms include: accretion onto the central star, viscous disk spreading, inner and outer disk truncation via stellar encounters, photoevaporation by stellar winds, the destructive stellar (UV and X-ray) radiation field, and the aggregation of material into orbiting planetary bodies (Hollenbach et al. 2000). The reservoir of circumstellar material initially present around a young T Tauri star is suspected to dissipate within 10^6 years on average, according to observations and stellar age tracks (Haisch et al. 2001; Bizzarro et al. 2005; Pascucci & Tachibana 2010), although there are also examples of disks possessing their primordial gas to ages beyond 10^7 years (see Favata et al. 1998); yet another indication that stellar age is not the primary determinant of the disk evolutionary state, as briefly hinted at in the last section. In fact, dusty disks around cooler (K and M type) PMS stars may live up to 2–3 times longer, meaning that dissipation mechanisms may not be as efficient in late-type stars (Sterzik et al. 2004; Carpenter et al. 2006; Lada et al. 2006), and that stellar properties other than age may still play a vital role in the disk lifetime.

When the envelope around a young forming star has dispersed, the revealed dust disk is usually several hundred AU in radius (Andrews et al. 2009; Isella et al. 2009; Ricci et al. 2010b). It is also about 5% of the mass of the central source (Andrews & Williams 2005; Fang et al. 2009; Greaves & Rice 2010), although a two-magnitude scatter in the derived disk masses ($\sim 0.1\,M_\odot$ to $\lesssim 0.001\,M_\odot$) has been observed around T Tauri stars (Beckwith et al. 1990). The ratio of the mass located in the disk versus the envelope can be used to distinguish between different YSO evolutionary stages (see Jørgensen et al. 2009), with this ratio increasing for more evolved systems. Thus, the disk masses observed likely represent the typical range possible from the time the disk is revealed until its disappearance. Another possibility is that some disks are more massive to begin with and as a result might easily survive longer, allowing more time for planet formation to occur (Andrews & Williams 2007). Indeed, some models show that a larger disk mass can result from a faster intrinsic rotation rate during the early disk accretion phase (see Visser & Dullemond 2010). And there is yet more evidence to support the idea that other initial conditions, like the composition of the disk, could also play a significant role in planet formation. For example, a higher disk metallicity to start out with (or roughly speaking, more dust to gas) may

quicken the planet formation process. Exoplanet statistics exhibit a trend toward higher occurrences of gas giants around metal-rich stars (Santos et al. 2003). Computer simulations are able to show that the higher concentration of metals in the early disk allow for the build-up of planetary cores before dispersal of the gas reservoir is possible, making gas giants more likely (Ida & Lin 2004; Johansen et al. 2009; Ercolano & Clarke 2010). In contrast, lower metallicities in star-forming regions in the extreme outer Galaxy are believed to contribute to the relatively rapid dispersal of the circumstellar disks seen there, possibly caused by lower UV extinction from small dust grains (Yasui et al. 2009). For these reasons, there is a need to compare the evolution of the gas reservoir relative to the dust, which is one of the main motivating factors for part of the research presented in this thesis.

Separate Dust and Gas Dispersal Mechanisms

In general, the disk mass is comprised of one part sub-micron-sized (carbon and silicate) dust grains and ninety-nine parts cold gas (primarily H, H_2, and He); a standard ratio that also characterizes the interstellar medium. However, high-resolution observations together with modeling of large gaseous disks have shown that considerably different dust-to-gas ratios may also make for reasonable fits to the data for some sources (see Dutrey et al. 2003; Panić et al. 2008; Thi et al. 2010). In addition, the outer disk regions can exhibit larger dust depletion with respect to the inner radii (e.g. van Kempen et al. 2007; Isella et al. 2007; Panić et al. 2009). In some cases, modeling the outer disk density profile with a tapered edge can resolve this "observational discrepancy" (see Hughes et al. 2008). Thus, whether the different dust-to-gas ratios are a direct result of the initial conditions, an evolutionary outcome, or an observational effect often remains to be disentangled, but the true underlying amount of available gas is crucial to the ability to form gas giant planets like Jupiter, and worthy of investigation. Unfortunately, far less is known about the molecular gas reservoir because it is significantly more difficult to observe than the dust (see Section 1.2.3). As a result, current disk modeling methodologies usually assume that the gas structure accurately traces the dust structure, even though one of the big open questions in protoplanetary disk research today is whether the separate dust and gas components evolve simultaneously?

Recent progress is being made to identify relevant trends in the physical and chemical evolution of the gas disk (e.g. Dutrey et al. 1997; Qi 2001; Dutrey et al. 2007; Panić & Hogerheijde 2009; Bergin 2009; Öberg et al. 2010). The results are revealing disks with markedly different gas and dust structures. Some of these studies confirm separate outer dust and gas radii (e.g. van Kempen et al. 2007; Panić et al. 2009), or find that cleared inner dust gaps can still retain their gas component (e.g. Brown et al. 2008; Boden et al. 2009), or indicate that the gas temperature structure may be decoupled from that of the dust (e.g. Panić et al. 2008), or even that the gas disk can be flared while the dust disk is self-shadowed (see Fedele et al. 2008). Additional analyses of the gas component—the primary target of two of the observational studies presented in this thesis—can shed light on the processes relevant to both the dust and gas dispersal, and how they might be coupled. In the meantime, we continue reviewing the current disk evolutionary picture, acknowledging that much of our present knowledge is still based primarily on observations of the dust content in disks.

An Overview of Disk Evolution from Dust Observations

Disks come in many shapes and sizes, primarily reflecting different evolutionary stages. They usually start out flared as they funnel material from the spherical rotationally-flattened envelope down onto the central star. With a flared geometry, they intercept more of the stellar light, directly heating (and ionizing) the upper disk layers, which then re-radiate thermal energy into the deeper layers below, helping to maintain a warmer internal disk temperature and a larger pressure scale height. Over time, all disks evolve toward increasingly flatter geometries when: the envelope that feeds the disk dissipates and ceases

to rain down on the disk; viscous spreading expands the disk material outward indefinitely while conserving angular momentum; the luminosity generated by the slowing accretion decreases, thus reducing the disk temperature and scale height; grain growth leads to a concentration of larger particles in the disk midplane; and, the disk evolves from a warm optically thick disk to a cold optically thin one (Dullemond & Dominik 2004a,b). During this flattening, disk clearing is likely to occur from the inside-out, initially forming an inner dust gap before dispersing the rest of the disk material via stellar photoevaporating winds, X-ray photoionization, UV photodissociation, and possibly via the process of planet formation itself (Strom et al. 1989; Skrutskie et al. 1990; Hollenbach et al. 2000).

By 3–8 Myr, only 10% of T Tauri stars still exhibit evidence for inner accretion disks (Hillenbrand 2005), a fact that may leave them more vulnerable to the stellar radiation field without the added veiling provided by accretion flows. From this point forward, the dissipation process appears to occur quite rapidly, within another 10^4–10^5 years by some estimates (Simon & Prato 1995; Wolk & Walter 1996), based on the fact that statistically fewer objects are observed in the transitional stage from CTTS to WTTS (Strom et al. 1989). However, the Spitzer Space Telescope (SST or Spitzer), launched in 2003, is quickly altering the field of transitional disks with observations at near- and mid-infrared wavelengths, and new analyses report that this transition period could be as long as 1 Myr (see Cieza et al. 2007; Currie & Kenyon 2009). In the meantime, a similar lack of statistical evidence for objects with an outer disk-in-transition suggests that the disk could be depleted throughout relatively simultaneously (Andrews & Williams 2005; Alexander & Armitage 2007; Alexander 2008). In further support, a recent study of grain growth signatures tracing both the inner and outer disk also revealed a parallel, albeit tentative, indication that the dust in disks might evolve concurrently at all radii (see Lommen et al. 2010). On the other hand, this initial finding stands in stark contrast to models that predict faster grain growth closer in to the forming star (Dullemond & Dominik 2004b; Natta et al. 2007), and follow-up studies have been unable to confirm the initial trend (Ricci et al. 2010a). In addition, several new observational studies are providing the first indications for a radial variation in the dust properties of individual sources (e.g. Isella et al. 2010; Banzatti et al. 2010). Consequently, a bi-modal interpretation of the observational data has been proposed (e.g. Strom et al. 1989; Cieza et al. 2007), contrasting transitional disks with inner holes versus those that are depleted homologously (see Cieza et al. 2007; Currie & Kenyon 2009; Ercolano et al. 2010; Merín et al. 2010). Therefore, it is important to determine whether two separate groups do exist and whether they might represent different outcomes for disk evolution or even different routes toward the same outcome, if we want to correctly place all disks into one evolutionary sequence.

Inner disk clearing, which may be followed by the rapid dispersal of the disk, can also be a sign of successful planet formation. There are currently two dominant theories for gas giant planet formation, known as the core accretion and the gravitational instability models. The core accretion model is currently the favored theory (see Safronov & Zvjagina 1969; Pollack et al. 1996); and the subject of a separate study in this thesis. The theory explains how sub-micron-sized dust grains in the disk initially collide and stick together quickly and efficiently due to surface adhesion, or specifically by van der Waals force (see Dominik & Tielens 1997; Poppe et al. 2000; Blum & Wurm 2008). In agreement with theory, laboratory studies have successfully reproduced the efficiency of collisional growth up to millimeter-sizes (Colwell & Taylor 1999; Blum et al. 2002; Colwell 2003; Love & Pettit 2004; Langkowski et al. 2008; Colwell et al. 2008). The collisions are caused by non-zero relative velocities due to turbulence and the differential coupling of the dust to the large-scale gas motions (Weidenschilling & Cuzzi 1993; Beckwith et al. 2000). When the growing dust agglomerate is massive enough ($\gtrsim$ 5–10 $M_\oplus$), a planetary core has formed and it is able to gravitationally accrete molecular gas. Runaway growth proceeds as the protoplanet sweeps up material in its orbital path until it has cleared a wide gap in the disk. At this point, several big challenges to the model appear during the intermediate growth stage. While collisional sticking is effective for small grains, and gravitational attraction works well for large boulders, the processes governing the growth of intermediate-sized grains (from millimeter sizes on up to kilometer

sizes), remains an open investigation (see Blum 2010, for a recent review). Theory predicts that turbulence in disks and the weak molecular bonds mean that collisions of millimeter-sized aggregates are prone to particle fragmentation and semi-elastic (or re-bounding) collisions (Schäfer et al. 2007; Paszun & Dominik 2009). Now new microgravity experiments confer (Chapter 7, Salter et al. 2009; Heißelmann et al. 2010). Subsequently, collisional growth appears to be an incomplete solution thus far for planet formation (Blum 2010). Recently, streaming instabilities have been invoked to aid the core accretion process (Johansen et al. 2009). The theory describes how eddies in the rotating Keplerian velocity field of the gaseous component collect dust particles allowing them to aggregate to larger sizes in lower-velocity collisions more easily. In addition, when collisions do result in fragmentation, the fragmented material does not escape the eddy, but rather falls back onto the accreting core. These spiral streams are able to explain the spin rates and propensity for prograde rotation of the small bodies in the Solar System (Johansen & Lacerda 2010). However, the instabilites then also inherently stipulate that sufficient gas surface densities must be available to overcome destructive growth processes, even during the formation of small rocky Earth-like planets.

In the end, the requirements that must be met for a successful planetary outcome can be summarized as: a large reservoir of both dust and gas, a longer gas disk lifetime than the timescale needed for a planet to form, effective grain growth mechanisms, and eventually, stable planetary orbits. In this context, this thesis addresses research including: observations to identify gas-rich disks toward massive dust disks, studies to probe destructive gas processes in disks exhibiting preliminary grain growth, and experiments probing the effectiveness of collisional growth processes at intermediate grain sizes.

1.2 The Study of Protoplanetary Disks

The majority of the analyses and results presented in this thesis are based on observations combined with modeling. Because the evolutionary timescales for disks are very long, on the order of several Myr, we use statistical surveys of many circumstellar disks (at presumably different evolutionary stages) to piece together the complete evolutionary timeline for a typical disk. Observations are easiest to make of sources in the nearest low-mass star-forming regions. This includes the Taurus-Auriga complex (140 pc, Kenyon et al. 1994), the Orion Nebula (440 pc, Hirota et al. 2007), and ρ Ophiuchus (135 pc, Mamajek 2008). In this thesis, our source observation lists are comprised almost entirely of low-mass objects in Taurus. In general, we justify this selection criterium by the intent to establish a uniform sample, located in a roughly identical environment, and possessing similar initial conditions; the caveats of Section 1.1 notwithstanding. This can tell us a great deal about the T Tauri population in Taurus, but may require some caution when extrapolating the results to the general low-mass stellar population because Taurus has several distinguishing characteristics that set it apart from other regions, including an unusually high stellar multiplicity rate ($\sim$75%), fewer high-mass stars, distributed (versus clustered) star formation, and a slightly higher disk fraction in general (Ghez et al. 1997; Luhman et al. 2010). Although some recent studies report that the dust properties seem to be independent of the star-forming region, suggesting that a more universal application of the results may also be possible (e.g. Lommen et al. 2010; Ricci et al. 2010a). In this section, we discuss our methods for studying the evolution of protoplanetary disks, including the telescope facilities used, the emission processes traced with observations, the disk (dust and gas) modeling, and finally, when we can study disk evolutionary processes in the laboratory.

1.2.1 Millimeter-wave Instrumentation

In Taurus, typical disk temperatures can range from 10 K in the midplane to 300 K in the surface layers. The importance of millimeter emission to probe such cold, dark and dense regions has been noted already, but making the transition to observations at longer wavelengths required new technological developments

in millimeter-wave instrumentation. For one thing, larger telescopes are necessary because the angular resolution is inversely proportional to the observed wavelength ($\sim 1.2\,\lambda/D$). For example, the IRAM 30-meter telescope (in Chapter 6) is the second largest millimeter dish in the world, while (in Chapter 2) the James Clerk Maxwell Telescope (JCMT), located on Mauna Kea in Hawaii, possesses a 15-meter dish diameter. At wavelengths of 1–3 mm, where the bulk of the cold disk material emits thermal radiation, the angular resolution (or beam-size) of each telescope ranges from 8–25″ and 17–50″, respectively. In contrast, an average protoplanetary disk of radius 500 AU in Taurus has an angular size of 7″ and fills just 72–8% and 17–2% of the respective beams, assuming a face-on disk orientation. Thus, no disk is ever resolved, and building larger telescope dishes that are still maneuverable, is technologically challenging. As a result, single-dish millimeter data typically suffer from low-resolution, beam dilution, pointing errors, absolute flux calibration errors ($\sim 20\%$), and in crowded regions, confusion from nearby sources that also fall within the beam. The telescopes are, however, well suited for large surveys of protoplanetary disks, like those in Chapters 2 and 6 of this thesis. In doing so, separate offset observations are now made toward nearby "empty" patches of the star-forming cloud to quantify the external contribution from dust and molecules (see Figure 2.4) in the surrounding environment and along the line-of-sight to each source (e.g. Thi et al. 2001; van Kempen et al. 2007). Still, continuum fluxes can provide only a lower limit to the dust mass when $R_{\rm dust}$ (or the amount of beam dilution) is unknown. And while gas-line observations can help us to search for trends in the disk chemistry (see Chapter 2) and constrain some disk parameters including the gas disk size $R_{\rm gas}$ and inclination i (e.g. Panić et al. 2008), a lot of the kinematical information is still lost. Ultimately, our goal is to resolve the radial variations and evolution of the gas, particularly in light of the evidence for both inside-out and homologous dust dispersal processes. Thus, having identified suitable disks for follow-up studies, it is necessary to seek out solutions to bigger telescopes yet.

To achieve higher angular resolution, millimeter-wave instrumentation has borrowed on the principle of radio interferometry to link together multiple millimeter dishes (or antennas) to create a larger collecting area. Modern facilities include the Combined Array for Millimeter-wave Astronomy (CARMA) in eastern California, the IRAM Plateau de Bure Interferometer (PdBI) in the French Alps, the Submillimeter Array (SMA) on Mauna Kea in Hawaii, and the Nobeyama Millimeter Array (NMA) in Japan. The next-generation Atacama Large Millimeter / submillimeter Array (ALMA), the only dedicated millimeter interferometer to be located in the southern hemisphere, is currently in its commissioning phase (see Figure 1.3). In the meantime, the interferometers operating today feature baselines of several hundred meters in length and resolutions of $\sim 0.5''$ (about 70 AU at the distance to Taurus); ALMA will extend this down to $0.02''$ (or 3 AU) at the same wavelengths. Several non-trivial performance enhancements are achieved while using interferometry techniques: increased collecting area improves sensitivity and the ability to detect smaller column densities of molecular gas, in addition to smaller dust mass (also at larger radii); longer baselines increase the angular resolution allowing us to probe the radial and vertical structure on smaller scales; and, the interferometer is more sensitive to compact disk emission because it resolves out (or does not efficiently detect) the large-scale extended envelope and cloud contributions that contaminate (and sometimes dominate) the single-dish data. Interferometric observations of protoplanetary disks can be very time-consuming to achieve adequate signal-to-noise, often lasting the entire 8–9 hours that a source remains visible over an array. An entire 8–9 hour track is also recommended for better image fidelity, which is defined by a combination of the source brightness distribution on the sky, the details of the u,v-coverage (or collecting area) of the antennas, and the de-convolution algorithm used when re-constructing the image from a sparsely sampled u,v-plane (see Taylor et al. 1999, for a detailed introduction to interferometry techniques).

While an interferometer approximates a telescope the size of its longest baseline, the combined telescope has many "holes" in it, which results in lost source information. Thus, the more u,v-coverage, the fewer the holes. This can be achieved in two ways, through a higher density of antennas or a longer

Figure 1.3 — An artist's drawing of the original vision for the Atacama Large Millimeter / submillimeter Array (ALMA), now in its commissioning phase. Located at the Chajnantor plateau in the Atacama desert in Chile, early science is slated to begin in late 2011 when the first 16—of the planned 66—antennas are online. (*Credit: ESO*)

observation. The latter strategy is effective because the u,v-sampling changes as the Earth rotates, filling in the u,v-plane (see Figure 1.4 for an illustration of this effect); in addition, the u,v-plane is more symmetrically sampled (producing a more circular beam). This was the guiding principle when defining our CARMA observing strategy in Chapter 3. Rather than observing two sources per night for four consecutive hours each, we chose to rotate through all of our sources repeatedly over the course of five nights. The result was the anticipated, quiescent 5-night light curve for all sources, except one! This serendipitous discovery of atypical millimeter activity toward a T Tauri source is the subject of Chapter 4 of the thesis (Salter et al. 2008). In the follow-up observations of Chapter 5, we continued to use the increased sensitivity of the CARMA, IRAM PdBI, and SMA interferometers to detect the small- and large-scale flux variations in the active millimeter light curve (Salter et al. 2010).

1.2.2 The Dust

Although the gas content dominates the disk mass, it is the dust content that dominates the observed emission at millimeter wavelengths. In this section, we cover how we can derive the large-scale dust structure from continuum observations, and then we summarize the diagnostics available to "zoom-in" on the small-scale processes that constitute the first steps of planet formation.

Circumstellar dust irradiated by the central source emits at a characteristic wavelength corresponding to its temperature, size, and emissivity properties. The summation of this thermal emission from all of the small dust grains in the disk defines a spectrum of total flux per wavelength known as the dust continuum. This is just one component of the source's Spectral Energy Distribution (SED), which also includes the stellar blackbody spectrum. Ranging from the near-infrared to radio wavelengths, the dust continuum represents one of the easiest disk diagnostics to measure. In addition, if the stellar *input*

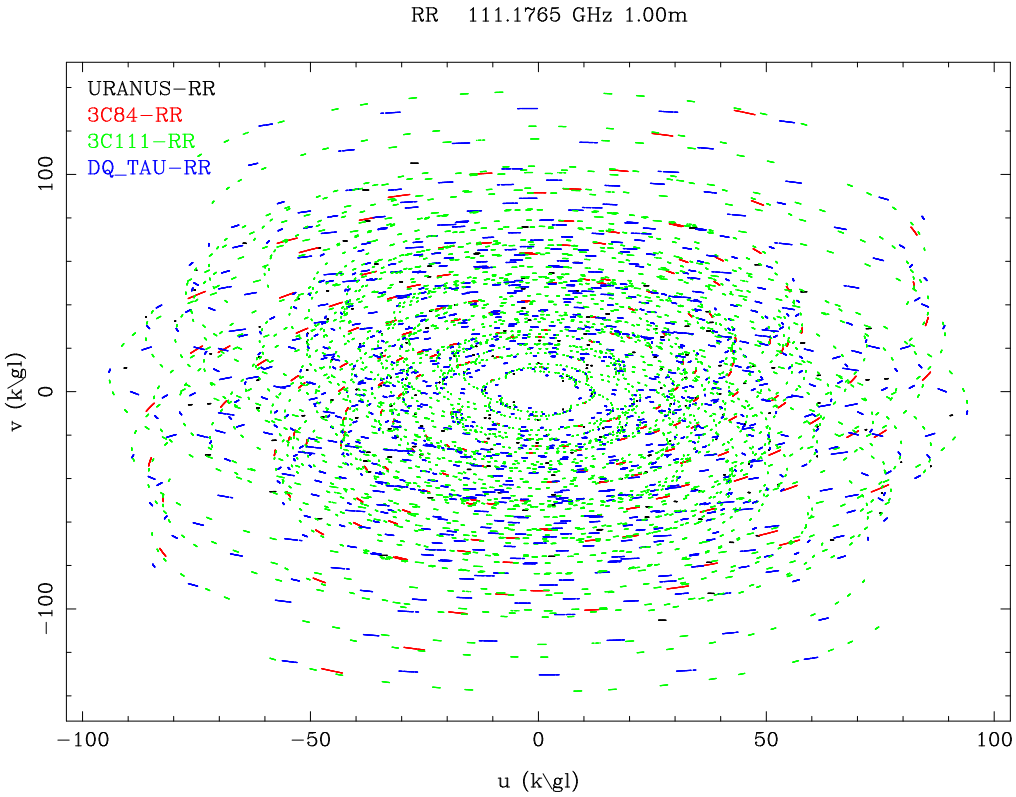

Figure 1.4 — The u,v-coverage for our CARMA C track on 2008 April 19 (see Chapter 2). The shorter (green) line segments represent the sampling for our 5-minute 3C 111 calibrator observations, while the longer (blue) segments are for each 12-minute DQ Tau on-source observation, and the longest (red) segments are the 3C 84 flux calibrator. Each grouping of nearly connected segments tracing out a curved path, represents one of the 120 baselines. For example, the arc running from $(-60,-110)$ to $(75,-110)$ shows that we observed 3C 111 fifteen times and DQ Tau five times throughout the track. The oval pattern in the coverage map is created by the rotation of the Earth during the course of a 8-hour track; each baseline will trace out an ellipse over the course of 24 hours.

radiation field (defined by $R_\star$, $L_\star$, and $T_\star$) is known, we can use dust radiative transfer calculations to reverse engineer the *output* SED and derive the temperature and density distribution of the circumstellar dust content (e.g. Dullemond & Turolla 2000). In Figure 1.5, we illustrate how four distinct SED shapes correspond to different circumstellar dust structures. In general, emission at shorter infrared wavelengths results from the warm surface layers and material closest to the star, whereas emission at longer radio wavelengths originates in the midplane and cold outer disk. As a result, when one or both of these regions is depleted of its dust, the corresponding emission is reduced, altering the SED shape. This process for deriving the large-scale dust structure is called SED modeling, and one of the biggest conclusions to be drawn from these analyses is, how the millimeter excess in particular is an important tracer of the disk structure information *and* therefore the total dust mass. With a few assumptions about the disk properties (i.e. radial size, mean dust temperature T, dust opacity κ_ν, and source distance D), a basic mass-flux relation ($S_\nu = 2\,k\,T\,\nu^2\,\kappa_\nu\;M_{\rm dust}\,/\,D^2\,c^2$) can be derived (see Beckwith et al. 1990; Dutrey et al. 1996).

SED modeling is not without its challenges, most notable of which is that the dust solutions are highly degenerate, meaning that many valid solutions exist for one SED profile. Additional constraints on the dust distribution can be made with millimeter interferometers when resolved observations detail the radial variation in the flux, in addition to the total integrated flux (e.g. Testi et al. 2001; Isella et al. 2009). In this respect, deriving the disk dust structure can be a very complicated and time-consuming

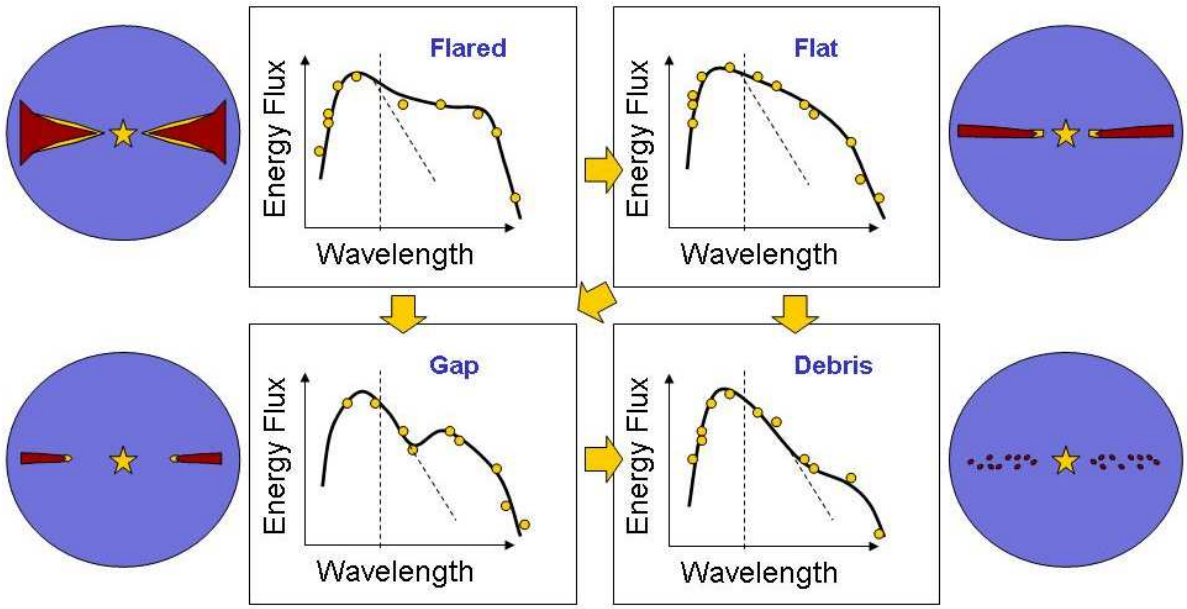

Figure 1.5 — A schematic illustrating how the spectral energy distribution (SED) of a source relates to the underlying dust structure. For example, disks with more mass, like the Flared or Flat disks, possess larger excesses at longer wavelengths. Whereas disks with inner holes, or the Gap disks, are characterized by dips at shorter wavelengths. Finally, we used arrows to indicate the potential routes for the evolution of one disk into another.

process involving many free parameters. Since there are many established dust models already available in the literature (e.g. Dullemond 2002; Dullemond et al. 2007; Robitaille et al. 2006), it is not our goal here to repeat the dust analysis. Instead, our motivation is to analyze the molecular gas content, and only then comment on the results within the context of the dust evolutionary state.

The SED profile is influenced most by the large-scale dust structure, but it can also reveal information about the current success of planet formation in the disk. One of the free parameters in the radiative transfer equations is the grain size. Larger particles intercept less radiation per unit volume, and therefore maintain colder core temperatures. Their peak thermal emission continues to shift toward longer wavelengths, until they have grown too large to efficiently radiate at millimeter wavelengths (Tanaka et al. 2005). When sufficient grain growth is occurring in the cold outer disk regions, the millimeter spectral slope will become shallower (Rodmann et al. 2006; Natta 2008; Lommen et al. 2010). Disentangling this effect due to growth from other evolutionary processes (e.g. mass loss) is trickier, but radio interferometry studies are able to confirm growth to at least a few centimeters in size (e.g. Wilner et al. 2000, 2005; Testi et al. 2001, 2003; Lommen et al. 2009), and in the case of TW Hya, predict that as much as $10^{-3}\,M_{\odot}$ could be hidden in large particles. At shorter wavelengths, the infrared regime allows us to probe grain growth in the warm surface regions of the disk. In recent years, the IRS instrument on board Spitzer has enabled astronomers to obtain the first mid-infrared spectra toward a large sample of PMS stars in Taurus (see Kessler-Silacci et al. 2006; Furlan et al. 2006). An analysis of the mid-infrared spectral slopes indicates again how shallower values are associated with grain growth and particularly dust settling. Just like in the cold outer disk regions, strong evidence for grain growth to centimeter sizes in the warm surface regions of the disk is found (e.g. Furlan et al. 2006). Finally, one additional diagnostic for grain growth in disks is the 10μm silicate emission feature. In those same Spitzer studies,

strong evolutionary markers have been identified whereby the strength and shape of the 10μm silicate feature decreases with a depleting population of small sub-micron-sized grains.

In this section, we have identified four main diagnostics that we can use to describe the current dust evolutionary state in our disk samples. They include: millimeter flux as an indication of the total available dust mass; the millimeter spectral slope as a probe of grain growth at large radii; the infrared spectral slope to identify grain growth at smaller radii; and the 10μm (and 20μm) silicate emission feature as a tracer of dust settling in the upper disk layers. All these properties will affect the disk structure, opacity, and surface density, among other disk properties. Our goals now are to analyze the gas content for changes that are connected to this evolution in the dust content, which would suggest that the dust and gas evolve simultaneously.

1.2.3 Cold Gas

The gas in disks is significantly harder to observe than the dust continuum, but as already iterated, the gas represents the bulk of the circumstellar material and it is a critical ingredient in the formation of gas giants. In this section, we focus on the processes responsible for the gas-phase emission lines, the disk properties that they trace, and our modeling methods to derive the underlying chemical abundances.

The most abundant molecule in disks, and in the universe, is molecular hydrogen (H_2). Its symmetric structure, however, means that it lacks a permanent electric dipole moment and the corresponding rotational spectra, making it one of the most difficult molecules to observe (cf. Thi et al. 2001; Lahuis et al. 2007; Bitner et al. 2008). Instead, carbon monoxide (CO) is a logical alternative tracer of the cold gas. While its most abundant isotope ^{12}CO is a roughly constant 10^{-4} times less abundant (in number) than H_2 (Frerking et al. 1982; Lacy et al. 1994; Terzieva & Herbst 1998), it is a stable molecule once formed, easy to excite, and possesses the greatest number of strong rotational lines in the millimeter regime, making it one of the most accessible molecules to observations. However, in stark contrast to the dust, molecular line emission is restricted to discrete emission frequencies, and it can only be produced when the local (H_2) density is larger than the critical value for a particular transition. The required density is determined by the collisional pumping needed to offset the spontaneous radiative decay process. This means that molecular transitions with a high critical density can only produce significant emission in high density regions. These excitation properties, which make for fainter lines and more challenging observations, also provide a clever way to trace different density regions within the disk by using a variety of molecular species and rotational transitions. The ^{12}CO molecule is itself characterized by relatively low critical values, meaning that it is capable of tracing most disk conditions, from densities of about 10^{12} molecules per cm^{-3} in the disk midplane to 10^3 molecules per cm^{-3} at the disk surface. The unfortunate trade-off is that the brightest ^{12}CO lines, with the largest column densities, are then more likely to be optically thick, and so effectively we only probe the upper disk layers (Dutrey et al. 1996, 2003). In addition, processes including freeze-out onto grains can remove CO from the gas-phase in cold and dense regions, depleting its column density in the midplane. When possible, ^{13}CO or C^{18}O are often used in combination, as optically thinner tracers that are expected to probe the entire disk (van Zadelhoff et al. 2001).

Additional bright molecular lines that we will probe in our research include HCO^+, HCN, and CN. These molecules have H_2 abundance ratios of 10^{-8}–10^{-9} in molecular clouds (see Terzieva & Herbst 1998), but their ratios are expected to increase in the presence of a strong ionizing X-ray source, like near a magnetically active young star (Lepp & Dalgarno 1996; Aikawa & Herbst 2001; Glassgold et al. 2004). T Tauri stars also possess relatively intense UV radiation, which efficiently photodissociates HCN into its components H and CN (Lepp & Dalgarno 1996; Aikawa et al. 2002; van Zadelhoff et al. 2003). X-ray ionization and UV photodissociation are two of the main drivers of the gas chemistry and gas dispersal in disks. Now by choosing comparable transitions (in terms of excitation energy) from different molecules,

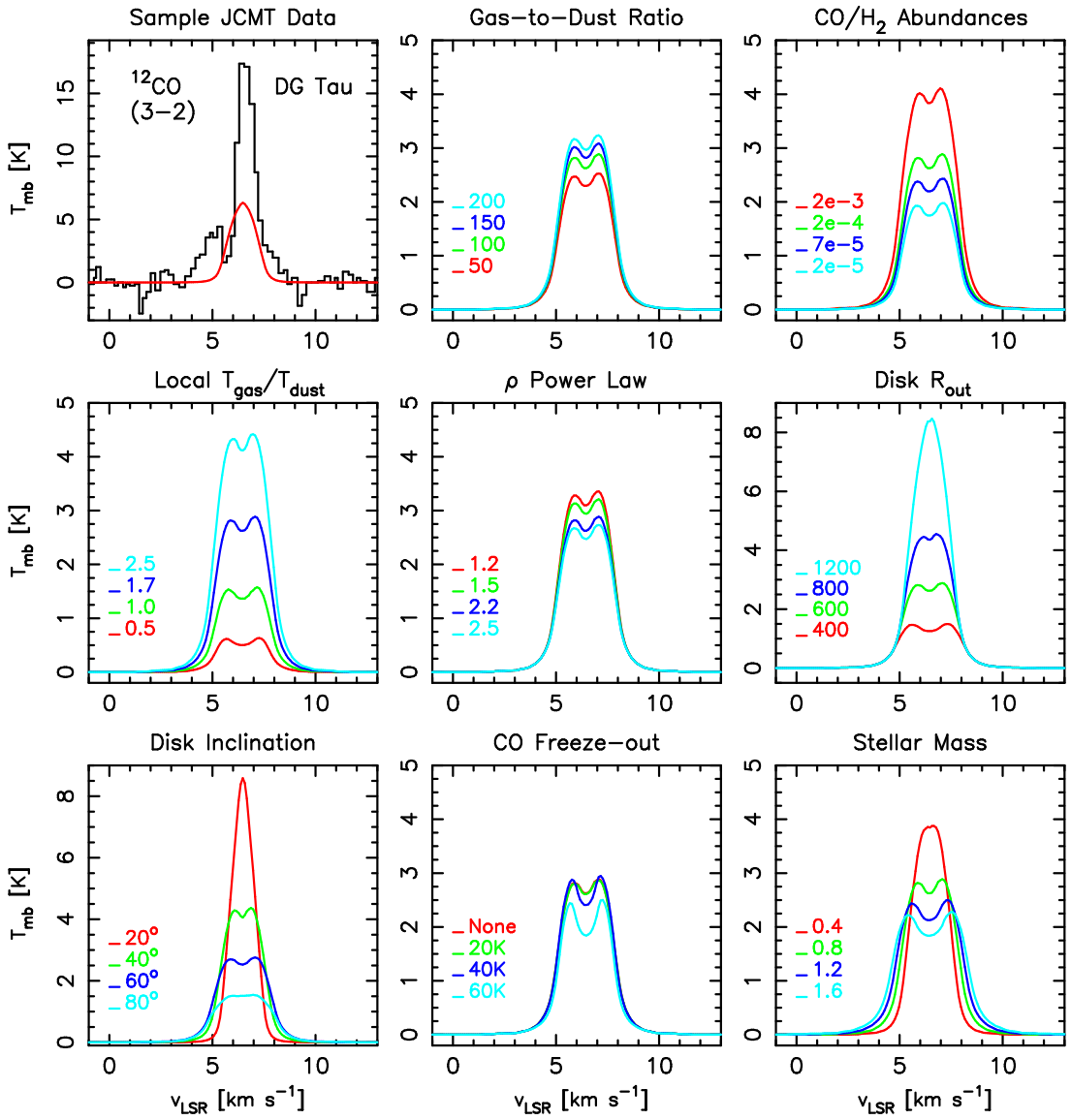

Figure 1.6 — Line models show how altering one parameter changes the predicted ^{12}CO (3–2) line profile for an unresolved disk. Shown from left to right, top to bottom (with default values in parentheses) are: the sample JCMT data and best fit for DG Tau showing contamination from bright cloud emission near $v_{\rm LSR} = 6.1\,{\rm km\,s^{-1}}$ and broad outflow wings (refer to Chapter 2), varying the dust-to-gas ratio (100), varying the CO/H_2 abundance ratio (2×10^{-4}), adjusting the gas kinetic temperature with respect to the local dust temperature (1.0), modifying the density power law (1.5), extending the disk to a different outer radii (600 AU), varying the disk inclination (60°), including CO freeze-out below different temperatures (no freeze-out), and altering the kinematical velocity profile by changing the central stellar mass ($0.8\,M_\odot$).

we can probe the same (or similar) disk region and look for variable molecular compositions that trace the level of X-ray ionization and UV photodissociation processing occurring in a uniform sample of disks (see Chapter 2). It is not our intent here to study the large chemical networks in disks, but rather, to apply those results to characterize the relative gas-phase content and chemical evolutionary state in similar disks.

Since several physical parameters of the gas disk may differ from the dust-defined disk structure, we show in Figure 1.6 how changing one parameter at a time alters the predicted line profile for an

unresolved disk. By far, the largest effects on the line intensity are the disk inclination and the outer gas radius, which is consistent with the fact that we detect larger gas disks in face-on orientations more often (Chapter 2). We can also see how, for example, the disk inclination and the central stellar mass are degenerate parameters, since both line profiles become stronger and narrower when these parameters are decreased. Similarly, we can increase the line intensity without affecting the line width by either increasing the gas-to-dust ratio or decreasing the density power law in the outer disk. These degenerative effects illustrate why it is challenging in single-dish data to derive the disk gas structure from the gas-line information alone. Resolved observations, on the other hand, allow us to extract the kinematics of the disk ($M_\star \sin i$), the outer radius ($R_{\rm gas}$), and the radial variation in the surface density; which also happen to be disk properties that are not accessible via dust observations. Unfortunately, modern interferometers can only resolve about 3–5 pixel elements across the face of most disks and only with very long-duration observations. This is where ALMA will have a dramatic impact on protoplanetary disk studies.

In the meantime, when we cannot directly compare the (radial and vertical) distribution of the gas and dust reservoirs, our strategy is to populate the solution for the dust structure with the canonical gas abundances, and then compare the resulting line predictions to the real data. A match suggests that the dust and gas structures are well coupled; a mismatch may indicate otherwise.

1.2.4 Relativistic Electrons

The study of synchrotron emission, or the signature radiation emitted by relativistic electrons spiraling along a magnetic field line, is usually restricted to the radio regime when studying PMS stars. There the electron energies involved are consistent with the surface magnetic field strengths typical of T Tauri stars (1–6 kG, or about 1000 times stronger than the Sun's field) (Basri et al. 1992; Johns-Krull et al. 1999). Thus, the discovery of transient high-energy non-thermal emission at millimeter wavelengths is of great interest, especially considering the presumed quiescent nature of the millimeter emission from disks. In this section, we review the role and impact of magnetic fields in T Tauri systems, and then shift our focus to magnetic interactions between stars in close-separation, high-eccentricity binary systems.

In a single CTTS scenario, the central source truncates the inner circumstellar disk in two ways. First, the stellar radiation field photoevaporates dust grains within a region where dust temperatures are ≥ 1500 K, creating a sharp inner dust edge. The second mechanism involves the radius at which material free-falls onto the star, and accretes. This is usually defined by the boundary where the magnetic field pressure is equivalent to the rotation pressure of the disk (governed by the gas kinematics). Within this corotation radius (at about 5 AU), the stellar magnetic field lines channel material onto the star; and beyond this boundary, the field lines become frozen to the Keplerian disk movements and act to slow the stellar rotation (Ghosh & Lamb 1978; Shu et al. 1994). These processes are the foundation of the magnetospheric accretion model, and in Figure 1.7 we illustrate the large-scale topological structure of the stellar magnetic field lines. As long as there is disk material at the co-rotation radius, the CTTS is expected to accrete at the observed rates of about 10^{-7}–$10^{-10}\,M_\odot$ per year (Hartigan et al. 1995; Gullbring et al. 1998). As the inner disk edge migrates outward over time, however, accretion may be halted. This occurs when the disk is photoevaporated from the inside-out or when material in the region is swept up into a protoplanet. At which point, the disk disperses rather rapidly, and the star begins to spin up (Bouvier et al. 1993, 1997). In this scenario, a rotationally generated stellar magnetic dynamo easily explains why a faster-spinning WTTS is even more magnetically active than a disk-bearing CTTS, as determined from X-ray surveys that credit the magnetic activity primarily to coronal reconnection events, or stellar flares (Stassun et al. 2006; Güdel & Nazé 2009).

Stellar flares, like solar flares, release magnetic energy when oppositely-directed field lines in the corona are forced together and re-connect to establish a more stable field configuration (Haisch et al. 1991, for a review). Reconnection is often associated with strong radio, optical, UV, and X-ray out-

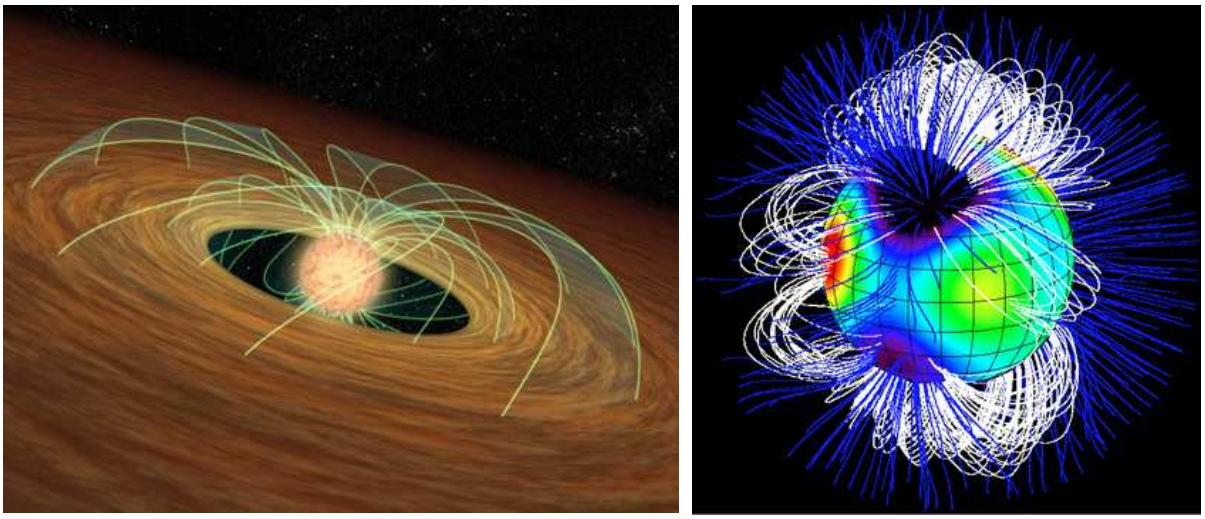

Figure 1.7 — At left, an artist's impression of the stellar magnetic field lines interacting with the circumstellar disk. Near the inner disk edge, material accretes onto the central star via the field lines. At larger radii, the field lines are tied to the disk motions, effectively slowing the stellar rotation. (*Credits: NASA / JPL-Caltech / R. Hurt of SSC*); At right, a topographical view of the magnetic field lines around the star τ Scorpii. Open field lines allow charged particles (and angular momentum) to be ejected from the system with the help of stellar winds. Closed loops indicate where charged particles can become trapped close to the star. (*Credits: ESPaDOnS / CFHT*)

bursts. The released magnetic energy is first converted to kinetic energy when charged particles in the region are accelerated, sometimes to relativistic speeds, and spiral down along the field lines emitting synchrotron radiation at radio frequencies. Then, when the charged particles collide with the stellar atmosphere at one of the two magnetic footprints, the particles heat and ionize the chromospheric plasma, resulting in optical, UV, and X-ray emission. In addition to these single-star magnetic events, other scenarios for reconnection include magnetic interactions between a star and its accretion disk, a star and a planet forming within its circumstellar disk, or a star and a stellar companion (Phillips et al. 1991). An interesting development from recent long-duration X-ray surveys is the once-a-week statistical occurrence of giant X-ray flares, which are consistent with T Tauri surface field strengths and coronal loop structures stretching to many stellar radii (Favata et al. 2005; Getman et al. 2008a,b). This presents an interesting scenario for close-separation binaries that can incur star-star magnetic field interactions (Massi et al. 2002, 2006, 2008; Salter et al. 2008, 2010, Chapters 4 and 5).

Since most stars form in multiple-star systems, there is an established need to study planet formation in these systems as well (Leinert et al. 1993; Simon & Prato 1995). Traditionally, the stellar dynamics were believed to effectively disrupt the disk and prevent stable planetary orbits. On the contrary, observational evidence for exoplanets have been found in a variety systems, including binary and triple systems (Raghavan et al. 2006), around primary host stars with both short- and long-period stellar companions (Chauvin et al. 2006; Eggenberger et al. 2007), and in circumbinary disks around close-separation (≤ 50 AU) binaries (Patience et al. 2002). However, tight binaries like the ones we study in this thesis, present additional challenges to planet formation. Theoretical models derive shorter disk lifetimes, primarily due to tidal truncation of the inner disks (Duchêne 2010), and observational studies show significantly reduced millimeter excess and accretion rates (Beckwith et al. 1990; Jensen et al. 1994). However, one open question in binary star research today concerns how some binaries can continue to accrete across large inner gaps when others cease. Some models are able to show how the dynamical motions in a high-eccentricity system can periodically perturb the outer circumbinary disk, causing material to flow in pulses towards the inner rim, overcoming the tidal barrier and accreting across

the gap (Artymowicz & Lubow 1996). We now recall how close binaries, or binaries with small periastron approaches, can experience star-star magnetic interactions. Thus, given the star-disk connection via the magnetospheric accretion model, we must question how a significant re-organization of the stellar magnetosphere might affect material in the disk where the open stellar field lines end. In other words, is it possible that reconnection events can assist, hinder, or explain pulsed accretion processes in these systems?

As it turns out, we can also study high-energy processes in the millimeter spectrum toward PMS stars. Relativistic electrons accelerated by powerful star-star reconnection events can allow us to sample T Tauri magnetic field strengths, sizes, and regeneration timescales. The potential impact for the circumbinary disk lifetime might include assisting or hindering accretion across gaps, extending viscous timescales, or removing more gas from the system through elevated levels of associated X-ray and UV activity. With regards to standard SED modeling of (unresolved) dust continuum fluxes, it should be cautioned that non-thermal contributions will adversely affect the best-fitting solution.

1.2.5 In the Laboratory

One additional way to study planet formation processes is in the laboratory. This requires re-creating the circumstellar disk conditions of a high vacuum ($\ll 10^{-2}$ mbar), cold temperatures (10–300 K), and a reduced-gravity ($\sim 0g$) environment. One additional caveat is that the physical process to be studied must be smaller than one's laboratory. In Chapter 7, this concerned a cylindrical vacuum chamber 110 mm high and 180 mm in diameter (Salter et al. 2009). The subject of the experiment is the collisional grain growth mechanism that currently forms the basis of the core accretion model for planet formation. In Section 1.1.2, we discussed the theoretical challenges to grain growth beyond centimeter sizes (e.g. Dominik & Tielens 1997; Paszun & Dominik 2009). In Chapter 7 we present the construction and early results of an experiment performed during a parabolic flight campaign organized by the European Space Agency (ESA). The flight maneuver simulates weightlessness for a period of 22 seconds (see Figure 1.8), thus achieving the longest duration reduced-gravity experience without going into space. Within this period,

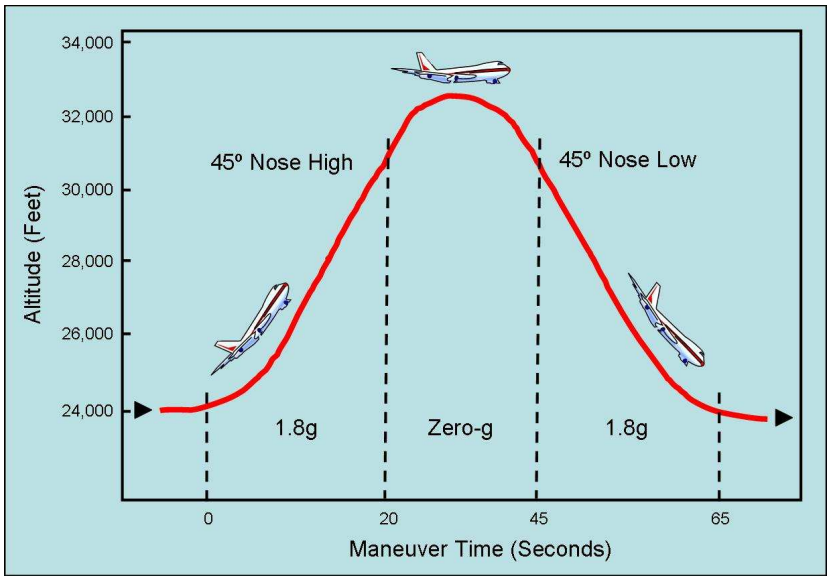

Figure 1.8 — A schematic of the flight profile during a parabolic flight campaign organized by the European Space Agency. A parabolic flight maneuver is just one way to approximate the zero-gravity conditions in a protoplanetary disk when performing experiments to test small-scale processes in disks in 22-second segments.

our goal was to execute several collisions of millimeter-sized protoplanetary dust analogs, and record with unobstructed views the outcome of each collision. This was best accomplished with single collision events, with the turnover time between events determined by the time needed to slowly accelerate each dust analog to the collisional velocity regime being investigated while preserving their porous structure. With the experiment setup defined in the last chapter, a broad range of particle sizes (from millimeter to centimeter), compositions (dust, ice, and dust-ice analogs), temperatures (80–300 K), and velocities (from 1.0–0.1 m s^{-1}) are capable of being studied. In this way, we can test in our own laboratories the small-scale planet formation processes occurring in disks many hundreds of parsecs away, and the same processes thought to be responsible for the formation of our own Solar System.

1.3 This Thesis

This thesis is split into three parts. In **Part I** of the thesis, we pursue observational clues from thermal emission processes to address what happens to the gas content in disks as the dust evolves. For example, in **Chapter 2** we examine specifically the effects that grain growth and dust settling have on the photoprocessing of the molecular gas (HCO^+, HCN, and CN) content. In **Chapter 3** we investigate the observational relationship between the CO gas-line measurements and the dust diagnostics. The studies in Part I are helping to identify the most (or least) influential processes driving the disk evolution, and to determine which of our current observational diagnostics are the most robust. **Part II** of the thesis emerged in the midst of observations for Part I, and it cautions against the long-standing notion that the millimeter flux observed toward young PMS stars is always dominated by the quiescent thermal emission from passively heated dust located in a circumstellar disk. In **Chapter 4** we report the serendipitous discovery of a transient millimeter flare toward the young spectroscopic binary DQ Tau; the first millimeter outburst to be documented toward a CTTS. In **Chapter 5** we confirm the recurring nature of the DQ Tau phenomenon. Then, in **Chapter 6**, we consider the proliferation of millimeter flares in a broader sample of young binaries targeted because their orbital parameters were similar to DQ Tau, and thus, presumably susceptible to the same phenomenon. As it turns out in Part II of this thesis, the monitoring of young pre-main-sequence binaries at millimeter wavelengths provides an interesting window into star-star magnetospheric interactions in binary systems. Finally, given the observational challenges present in the first two parts of the thesis, **Part III** documents a laboratory approach to investigate directly the coagulation theory of grain growth in protoplanetary disks. Described in **Chapter 7** are the technical details and initial scientific results of a parabolic flight experiment to study the low-velocity collisional properties of millimeter-sized dust particles. What follows now is a detailed overview of each chapter, concluding with the main results that can be drawn from each study.

1.3.1 Outline of Chapters

In **Chapter 2** we use HCO^+, HCN, and CN gas-line observations and modeling to search for increased photoprocessing effects when the small-grain population in the upper disk layers has been reduced via grain growth and dust settling. This study represents one of the few observational analyses of rarer molecular species toward a large, uniform sample of disks. Using the JCMT, combined with the line data already in the literature, we found no significant trends between the observed gas-line diagnostics (i.e. line strengths, ratios, and integrated fluxes) and either the dust diagnostics (i.e. silicate emission features, mid-infrared slopes, or 1.3 mm fluxes) or several stellar properties (i.e. $M_\star$, $L_{\rm bol}$, $L_{\rm X}$, or Hα EW). In other words, the expected molecular enhancements do not seem to correlate with the total dust mass or the presence of small grains in the inner and upper disk layers based on the observed line emission, which is most sensitive to the bulk of molecular gas in the outer disk (Figures 2.5–2.7). To derive the underlying (disk-averaged) molecular abundances, we used two different dust model prescriptions from the literature

to approximate the temperature and density structure of the gaseous component. The models struggle to reproduce the gas lines, mostly due to system parameters that are not well constrained by the SED (i.e. $M_\star$, i, $R_{\rm gas}$, and $T_{\rm kin}$) and instead represent just one combination of many suitable fits to the profile (Figures 2.8–2.9). We proceeded to model the source DG Tau in greater detail, discovering a reasonable fit to the gas-line data when $M_\star$, i, $R_{\rm gas}$, and $T_{\rm kin}$ were modified (Figures 2.10–2.11). The modeling of DG Tau illustrates the potential discrepancies between the line ratios as abundance tracers and the true underlying abundances, with the measured CN/HCN line ratio (> 12) a factor 13 less than the fitted underlying abundance ratio (> 160). Instead, resolved observations of both the dust and gas alike are necessary in order to contrast their evolution more completely.

We present, in **Chapter 3**, interferometric observations of ^{12}CO ($J = 1$–0) toward five bright CTTSs in Taurus that are presumed gas-rich (from their dust continuum emission); as well as supplementary ^{12}CO ($J = 2$–1) observations toward one of these sources. These observations complete the interferometric sampling of a CO rotational line toward Taurus disks with a 1.3 mm flux ≥ 75 mJy. We report CO emission from three sources, where all integrated spectra are characterized by narrow emission peaks with multiple components spread over a wide velocity range (< 12 km s^{-1}). We find no significant trends in the CO line intensity or detection statistics with any of the current diagnostics for the dust evolutionary state; both in our subsample and in the current literature. We conclude for four of the sources that the CO line profile is obscured by large amounts of optically thick CO along the line-of-sight, which appears as a common trend in most spatially resolved CO analyses. As a result, we caution that observations of the lowest rotational lines of CO are an incomplete tracer of the total gas content, and therefore not a good probe of the gas evolution. We recommend that future observations focus on higher rotational transitions of CO, particularly with ALMA when improved sensitivity capabilities will allow for the detection of these higher frequency transitions.

In **Chapter 4** we report the discovery of a millimeter flare toward the spectroscopic binary DQ Tau in the Taurus star-forming region. The 2008 April 19 detection is the *first* millimeter outburst to be observed toward a classical T Tauri star. The activity was recorded during a 5-day survey of the quiescent thermal emission toward several protoplanetary disks in Taurus using the CARMA array (see Chapter 3). While the other four sources maintained a quiescent flux throughout the survey, DQ Tau brightened on the third night to reach a maximum detected flux of 468 mJy, almost 27 times its quiescent value, within a 2-hour period (Figure 4.1). We attributed the emission to synchrotron radiation. The two stars have a minimum separation of 8 $R_\star$ at their closest approach, whereby their magnetospheres (of theoretical size 5 $R_\star$) are predicted to overlap (Mathieu et al. 1997; Basri et al. 1997). Since the peak of our observed flare occurred just 7.6 hours before periastron, we make a case for colliding magnetospheres and predict that the flare mechanism is linked to the binary orbit and therefore likely to repeat. We also remark that the millimeter activity of DQ Tau could be linked (strictly in timing or via magnetospheric accretion theory) to the variable accretion bursts that explain the source's optical variability. In a broader context, these findings present a significant cautionary tale for millimeter flux points in the SEDs used for disk modeling that could include non-thermal emission contributions if measured only once.

Chapter 5 is a natural follow-up to the initial DQ Tau flare analysis and its implications for millimeter-wave studies of protoplanetary disks. There we present light curves covering a period of 8–16 hours near three additional periastron encounters where we again detected excess flux at 3 mm (Figure 5.1). An analysis of the similar exponential decay profiles allows us to estimate an average flare duration of 30 hours (Figure 5.3). The consistent timing of the flares within a 22-hour window near periastron, corresponding to stellar separations of 8–13 $R_\star$, supports the periodic nature expected from a scenario for colliding magnetospheres (Figure 5.4). We are also able to constrain the main synchrotron emission region to a stellar height of 3.7–6.8 $R_\star$, or about half the stellar separation distance at the time of an event. Assuming a well-ordered dipole topology for each magnetosphere beyond a radius of 3.7 $R_\star$, we determine that the magnetospheres must be misaligned at a significant angle in order for the observed reconnection events

to occur (Figure 5.8). We also speculate on an interesting scenario for on-and-off periods of flaring if the magnetic axis of one of the stars was to flip, as occurs in the Sun every 11 years. Otherwise, assuming one 30-hour flare per orbit, DQ Tau could spend as much as 8% of its 15.8-day orbital period in an elevated flux state. In combination with these millimeter observations, we coordinated simulataneous optical (as well as X-ray, see Getman et al. 2010, submitted) monitoring of DQ Tau, which shows that accretion activity can occur coincident in both time and duration with the synchrotron fallout of a magnetic reconnection event (Figure 5.7). Whether a causal or co-dependent relationship between the reconnection and accretion processes is in effect remains undetermined. The potential for bi-weekly flares, on the other hand, exposes the disk to highly elevated levels of X-rays (perhaps up to 100 times brighter in peak luminosity Getman et al. 2008a) and UV radiation; levels that are more likely to destroy HCO^+ and CN rather than enhance their fractional abundances (Lepp & Dalgarno 1996). This probably contributes to the non-detection of both molecules in the JCMT spectra toward DQ Tau (Chapter 2). In this way, we highlight the unknown effects of the stellar magnetospheric activity on disk lifetimes and the destruction processes affecting the gas reservoir.

Chapter 6 considers the proliferation of millimeter flares toward young stars. Stars possess stronger magnetic fields and exhibit their highest levels of magnetic activity during the PMS stage, as documented by recent X-ray surveys (e.g Güdel et al. 2007; Getman et al. 2008a,b). Given the current evidence for colliding magnetospheres in the DQ Tau PMS binary system, as well as the favorable statistics for close-separation binaries, we conducted a targeted monitoring program of the millimeter emission toward a sample of young spectroscopic binaries using the IRAM 30-meter telescope; the first dedicated survey to search for millimeter variability toward PMS stars. The sample includes six binaries of high orbital eccentricity ($e \geq 0.1$) and six binaries with roughly circular orbits ($e \approx 0$). The second group serves as a control sample, since the magnetospheres are not expected to periodically re-organize if the separation distance between the stars is constant throughout the orbit. On the other hand, a statistically significant occurrence of flares in these systems, would suggest an alternative flare mechanism is responsible, or more prevalent. Over five consecutive nights, during which each of the six high-eccentricity binaries completed periastron, only one source displayed millimeter variability. The source, UZ Tau E, is the one that most resembles DQ Tau in terms of orbital parameters and optical accretion activity. We observed a flux range for the combined hierachical quadruple system UZ Tau of 107–199 mJy (see Figure 6.1). The sparsely-sampled light curve, which does not resolve the E and W components of this hierarchichal quadruple system but does cover a broad period around periastron, exhibits behaviors that were predicted in Chapter 5, such as a double brightening and a faster flux decay time at larger stellar separations. The component UZ Tau E appears to be highly variable based on many previous millimeter interferometric observations at different wavelengths, perhaps statistically indicative of activity at many different orbital phases. Therefore, we are unable to confirm definitively that the multiple brightenings observed in this system near one periastron are uniquely explained by colliding magnetospheres. Still, UZ Tau E does present a strong case for multi-wavelength follow-up observations similar to those of DQ Tau. It also suggests that millimeter activity may be more common among PMS stars.

In the final chapter, **Chapter 7**, we use a laboratory experiment to probe grain growth processes in disks. We specifically test the core accretion model for planet formation by colliding protoplanetary dust analogs together in a simulated disk environment. The experiment consisted of two scenarios. In the first, we began by firing individual aggregates at a large target of similar, but denser, dust structure to represent a collision with a larger particle. We then followed with collisions between similarly-sized aggregates. We recorded over 100 separate impacts at 107 frames per second during 33 minutes of combined weightlessness. The results of this warm dust experiment probing collisions of particles measuring 0.2–6 mm across and traveling at speeds of 16–18 cm s^{-1} in ambient temperatures (300 K), showed that the majority of collisions (roughly 80–90%) resulted in semi-elastic re-bounding events. On average, only 15% of the translational energy is conserved during most events, probably due to aggregate com-

paction. Sticking was observed in only 10% of the particle-target collisions, and fragmentation occurred in roughly 10% of the aggregate-aggregate collisions. These results seem to indicate a critical transition regime for the collision velocities of dust aggregates when interactions start to become more destructive than constructive. Follow-up experiments with icy particles, expected to possess stronger molecular bonds, indicate similar "transition-zone" results (see Heißelmann et al. 2010). Our laboratory results confirm the predicted challenges for the core accretion model when it comes to collisonal growth beyond millimeter-sized aggregates.

1.3.2 Main Results

This thesis covers three major topics in the field of protoplanetary research: 1. The evolution of the dust and gas content with respect to one another, as deduced from observational studies of thermal emission diagnostics; 2. The nature and proliferation of transient non-thermal millimeter flares; and 3. The collisional grain growth processes in protoplanetary disks. The main results of these studies can be summarized in the following bullet points:

- Observations of 21 disks in Taurus show no correlations between their HCO^+, HCN, and CN line fluxes or ratios (which trace ionization and photodissociation processes) and their mid-infrared slopes or 10μm silicate emission features (which trace successful grain growth and dust settling). Therefore, the properties and evolution of the regions that dominate the gas-line emission ($R \gtrsim 100$ AU) appear unrelated to the ($R \lesssim 30$–100 AU) regions probed by common tracers of the dust properties and evolution. (Chapter 2)

- Modeling of unresolved gas-line observations is unable to break the degeneracies in the dust model fits. We show for the gas-rich disk around DG Tau how two very different disk temperature and density profiles can produce very similar lines for the same fractional abundances. However, this does not, in turn, necessitate that the abundance estimate is robust. Therefore, gas-line measurements and resolved observations of the dust and gas alike are needed to arrive at the full picture. (Chapter 2)

- Observations of low-J rotational lines of CO toward the brightest ($F_{1.3\mathrm{mm}} \geq 75$ mJy) objects in Taurus reveal very different CO line intensities for dust disks with similar mass, grain growth, and dust settling properties. In addition, two sources that are equally bright in one CO transition line do not necessarily possess similar brightnesses in another transition. Almost all sources exhibit at least some level of obscuration from optically thick CO along the line-of-sight, accounting for some of these observational differences. We caution that low-J transition lines of the main CO isotopologue are often an incomplete tracer of the total gas content and disk dynamics, and therefore not a robust probe of the gas evolution. (Chapter 3)

- Millimeter flares in the DQ Tau PMS binary system ($d_{\mathrm{min}} = 8.1\,R_\star$, $e = 0.56$, and $P = 15.8$ days) are recurring and can be explained by synchrotron emission initiated by a magnetic reconnection event when the two stellar magnetospheres collide during periastron passage. The derived coronal loop sizes of $\sim$3–5 $R_\star$ and surface field strengths of $\sim$3 kG are consistent with T Tauri magnetospheric values and a reconnection site located halfway between the two stars. Consistent activity during 4 separate periastron encounters indicates that the DQ Tau magnetospheres are capable of regenerating their fields on a bi-weekly basis. (Chapters 4 and 5)

- We report that another PMS binary, UZ Tau E, shares similar orbital properties ($d_{\mathrm{min}} = 11.6\,R_\star$, $e = 0.33$, and $P = 19.1$ days) and tentatively exhibits comparable activity (brightens by a factor 2 on two separate occassions). Short-period, close-separation, and high-eccentricity binaries are most

likely to experience the same phenomenon, properties that characterize a large number of young stellar systems. (Chapter 6)

- Our flare statistics caution against the long-held notion of a purely quiescent millimeter spectrum and emphasize the need for better characterization of the millimeter variability towards young stars, particularly when relying on one-time millimeter flux measurements to derive the dust (spectral slope) properties and the underlying disk structure. While peak values like those seen toward DQ Tau ($\sim$0.5 Jy) are rarer—but more easily recognized—smaller increases of a factor 2–3 like those observed toward UZ Tau E may remain unnoticed and be more common. (Chapers 5 and 6)

- The collisional growth mechanism for dust (and ice) particles in disks becomes less effective as particles approach centimeter-sizes and 1 m s^{-1} velocities with $\sim$90% of our dusty aggregate collisions resulting in re-bounding events during our initial microgravity experiment. Our laboratory results, together with recent follow-up experiments and complementary theoretical models, suggest that an alternative growth mechanism must be invoked at the intermediate growth stages in order to achieve meter-sized boulders and runaway growth via self-gravity. (Chapter 7)

1.3.3 Outlook

One of the most exciting developments soon to hit the field of protoplanetary disks research at millimeter wavelengths is the newest revolution in astronomical instrumentation, and one of the most ambitious astronomy projects ever undertaken, and that is ALMA. The interferometric telescope will consist of no fewer than 66 individual antennas, defining 2016 separate baselines ranging 15–16,000 meters in length. The antenna receivers will operate at wavelengths of 0.3–9.6 mm, corresponding to 10 frequency bands spanning the 31–950 GHz range. ALMA is currently being constructed at the Chajnantor plateau in the Atacama desert in Chile, one of the driest regions on Earth at an altitude of 5000 m, which puts it above 50% of the Earth's atmosphere, drastically reducing the sky background noise levels. Early science is slated for late 2011 when the first 16 antennas are in place. The array, when complete, will possess an unprecendented combination of sensitivity, angular resolution, spectral resolution, and imaging fidelity (Kurz & Shaver 1999).

In the future, it is our goal to compare the radial gas variations and chemical abundances, which will help us derive better, more complete disk models; and extend our work in Chapters 2–3 (Part I). ALMA will help by drastically reducing the time required for large, multi-epoch surveys, and subsequently allowing us to better characterize any time-dependent millimeter variability toward young stars, as we have initiated in Chapters 4–6 (Part II) of this thesis. As far as identifying the first stages of planet formation, many simulations to date predict that ALMA has the potential to detect the tidal effects of embedded protoplanets in disks using continuum studies (Wolf & D'Angelo 2005), or use high-lying molecular transitions of HCO^+ (or any other dense tracer) to detect disk instabilities or clumpiness (Narayanan et al. 2006). Whereas we show in Chapter 7 (Part III) how the collisional growth mechanism for planet formation faces challenges in both theory *and* experiment, ALMA may provide more definitive, observational evidence to test the current planet formation theories. These are just a few highlights of the possibilities with ALMA, as related to the subjects presented in this thesis.

Bibliography

Aikawa, Y. & Herbst, E. 2001, A&A, 371, 1107
Aikawa, Y., van Zadelhoff, G. J., van Dishoeck, E. F., & Herbst, E. 2002, A&A, 386, 622
Alexander, R. 2008, New A Rev., 52, 60
Alexander, R. D. & Armitage, P. J. 2007, MNRAS, 375, 500

André, P., Ward-Thompson, D., & Barsony, M. 1993, ApJ, 406, 122
Andrews, S. M. & Williams, J. P. 2005, ApJ, 631, 1134
Andrews, S. M. & Williams, J. P. 2007, ApJ, 659, 705
Andrews, S. M., Wilner, D. J., Hughes, A. M., Qi, C., & Dullemond, C. P. 2009, ApJ, 700, 1502
Artymowicz, P. & Lubow, S. H. 1996, ApJ, 467, L77+
Aumann, H. H., Beichman, C. A., Gillett, F. C., et al. 1984, ApJ, 278, L23
Banzatti, A., Testi, L., Isella, A., et al. 2010, ArXiv e-prints
Baranne, A., Queloz, D., Mayor, M., et al. 1996, A&AS, 119, 373
Barge, P., Baglin, A., Auvergne, M., et al. 2008, A&A, 482, L17
Basri, G., Johns-Krull, C. M., & Mathieu, R. D. 1997, AJ, 114, 781
Basri, G., Marcy, G. W., & Valenti, J. A. 1992, ApJ, 390, 622
Basu, S. 1998, ApJ, 509, 229
Beckwith, S. V. W., Henning, T., & Nakagawa, Y. 2000, Protostars and Planets IV, 533
Beckwith, S. V. W., Sargent, A. I., Chini, R. S., & Guesten, R. 1990, AJ, 99, 924
Bergin, E. A. 2009, ArXiv e-prints
Bergin, E. A. & Tafalla, M. 2007, ARA&A, 45, 339
Bitner, M. A., Richter, M. J., Lacy, J. H., et al. 2008, ApJ, 688, 1326
Bizzarro, M., Baker, J. A., Haack, H., & Lundgaard, K. L. 2005, ApJ, 632, L41
Blum, J. 2010, ArXiv e-prints
Blum, J. & Wurm, G. 2008, ARA&A, 46, 21
Blum, J., Wurm, G., Poppe, T., Kempf, S., & Kozasa, T. 2002, Advances in Space Research, 29, 497
Boden, A. F., Akeson, R. L., Sargent, A. I., et al. 2009, ApJ, 696, L111
Bok, B. J. 1948, Harvard Observatory Monographs, 7, 53
Borucki, W. J., Koch, D. G., Lissauer, J., et al. 2007, in Astronomical Society of the Pacific Conference Series, Vol. 366, Transiting Extrapolar Planets Workshop, ed. C. Afonso, D. Weldrake, & T. Henning, 309–+
Bouchy, F., Pont, F., Santos, N. C., et al. 2004, A&A, 421, L13
Bouvier, J., Cabrit, S., Fernandez, M., Martin, E. L., & Matthews, J. M. 1993, A&A, 272, 176
Bouvier, J., Forestini, M., & Allain, S. 1997, A&A, 326, 1023
Brinch, C., Hogerheijde, M. R., & Richling, S. 2008, A&A, 489, 607
Brinch, C., Jørgensen, J. K., & Hogerheijde, M. R. 2009, A&A, 502, 199
Brown, J. M., Blake, G. A., Qi, C., Dullemond, C. P., & Wilner, D. J. 2008, ApJ, 675, L109
Butler, R. P. & Marcy, G. W. 1996, ApJ, 464, L153+
Carpenter, J. M., Mamajek, E. E., Hillenbrand, L. A., & Meyer, M. R. 2006, ApJ, 651, L49
Cassen, P. & Moosman, A. 1981, Icarus, 48, 353
Chandler, C. J., Carlstrom, J. E., & Terebey, S. 1994, in Astronomical Society of the Pacific Conference Series, Vol. 65, Clouds, Cores, and Low Mass Stars, ed. D. P. Clemens & R. Barvainis, 241–+
Charbonneau, D., Brown, T. M., Latham, D. W., & Mayor, M. 2000, ApJ, 529, L45
Chauvin, G., Lagrange, A., Udry, S., et al. 2006, A&A, 456, 1165
Cieza, L., Padgett, D. L., Stapelfeldt, K. R., et al. 2007, ApJ, 667, 308
Colwell, J. & Taylor, M. 1999, Icarus, 138, 241
Colwell, J. E. 2003, Icarus, 164, 188
Colwell, J. E., Sture, S., Cintala, M., et al. 2008, Icarus, 195, 908
Currie, T. & Kenyon, S. J. 2009, AJ, 138, 703
Dobbs, C. L., Bonnell, I. A., & Clark, P. C. 2005, MNRAS, 360, 2
Dominik, C. & Tielens, A. G. G. M. 1997, ApJ, 480, 647
Duchêne, G. 2010, ApJ, 709, L114
Dullemond, C. P. 2002, A&A, 395, 853

Dullemond, C. P. & Dominik, C. 2004a, A&A, 421, 1075
Dullemond, C. P. & Dominik, C. 2004b, in Astronomical Society of the Pacific Conference Series, Vol. 321, Extrasolar Planets: Today and Tomorrow, ed. J. Beaulieu, A. Lecavelier Des Etangs, & C. Terquem, 361–+
Dullemond, C. P., Hollenbach, D., Kamp, I., & D'Alessio, P. 2007, Protostars and Planets V, 555
Dullemond, C. P. & Turolla, R. 2000, A&A, 360, 1187
Duquennoy, A. & Mayor, M. 1991, A&A, 248, 485
Dutrey, A., Guilloteau, S., Duvert, G., et al. 1996, A&A, 309, 493
Dutrey, A., Guilloteau, S., & Guelin, M. 1997, A&A, 317, L55
Dutrey, A., Guilloteau, S., & Simon, M. 1993, Journal des Astronomes Francais, 45, 8
Dutrey, A., Guilloteau, S., & Simon, M. 2003, A&A, 402, 1003
Dutrey, A., Henning, T., Guilloteau, S., et al. 2007, A&A, 464, 615
Eggenberger, A., Udry, S., Chauvin, G., et al. 2007, A&A, 474, 273
Ercolano, B. & Clarke, C. J. 2010, MNRAS, 402, 2735
Ercolano, B., Clarke, C. J., & Hall, A. C. 2010, ArXiv e-prints
Fang, M., van Boekel, R., Wang, W., et al. 2009, A&A, 504, 461
Favata, F., Flaccomio, E., Reale, F., et al. 2005, ApJS, 160, 469
Favata, F., Micela, G., Sciortino, S., & D'Antona, F. 1998, A&A, 335, 218
Fedele, D., van den Ancker, M. E., Acke, B., et al. 2008, A&A, 491, 809
Frerking, M. A., Langer, W. D., & Wilson, R. W. 1982, ApJ, 262, 590
Furlan, E., Hartmann, L., Calvet, N., et al. 2006, ApJS, 165, 568
Getman, K., Broos, P. S., Salter, D. M., Garmire, G. P., & Hogerheijde, M. R. 2010, submitted, ApJ
Getman, K. V., Feigelson, E. D., Broos, P. S., Micela, G., & Garmire, G. P. 2008a, ApJ, 688, 418
Getman, K. V., Feigelson, E. D., Micela, G., et al. 2008b, ApJ, 688, 437
Ghez, A. M., McCarthy, D. W., Patience, J. L., & Beck, T. L. 1997, ApJ, 481, 378
Ghosh, P. & Lamb, F. K. 1978, ApJ, 223, L83
Glassgold, A. E., Najita, J., & Igea, J. 2004, ApJ, 615, 972
Goodman, A. A., Benson, P. J., Fuller, G. A., & Myers, P. C. 1993, ApJ, 406, 528
Greaves, J. S. & Rice, W. K. M. 2010, MNRAS, 1110
Güdel, M., Briggs, K. R., Arzner, K., et al. 2007, A&A, 468, 353
Güdel, M. & Nazé, Y. 2009, A&A Rev., 17, 309
Gullbring, E., Hartmann, L., Briceno, C., & Calvet, N. 1998, ApJ, 492, 323
Haisch, B., Strong, K. T., & Rodono, M. 1991, ARA&A, 29, 275
Haisch, Jr., K. E., Lada, E. A., & Lada, C. J. 2001, ApJ, 553, L153
Hartigan, P., Edwards, S., & Ghandour, L. 1995, ApJ, 452, 736
Hayashi, C. 1961, PASJ, 13, 450
Hayashi, C., Hō̄shi, R., & Sugimoto, D. 1962, Progress of Theoretical Physics Supplement, 22, 1
Heißelmann, D., Blum, J., Fraser, H. J., & Wolling, K. 2010, Icarus, 206, 424
Henry, G. W., Marcy, G. W., Butler, R. P., & Vogt, S. S. 2000, ApJ, 529, L41
Herschel, W. 1785, Royal Society of London Philosophical Transactions Series I, 75, 213
Hillenbrand, L. A. 2005, ArXiv Astrophysics e-prints
Hirota, T., Bushimata, T., Choi, Y. K., et al. 2007, PASJ, 59, 897
Hogerheijde, M. R. 2001, ApJ, 553, 618
Hollenbach, D. J., Yorke, H. W., & Johnstone, D. 2000, Protostars and Planets IV, 401
Hughes, A. M., Wilner, D. J., Qi, C., & Hogerheijde, M. R. 2008, ApJ, 678, 1119
Ida, S. & Lin, D. N. C. 2004, ApJ, 616, 567
Isella, A., Carpenter, J. M., & Sargent, A. I. 2009, ApJ, 701, 260
Isella, A., Carpenter, J. M., & Sargent, A. I. 2010, ApJ, 714, 1746

Isella, A., Testi, L., Natta, A., et al. 2007, A&A, 469, 213
Jensen, E. L. N., Mathieu, R. D., & Fuller, G. A. 1994, ApJ, 429, L29
Johansen, A. & Lacerda, P. 2010, MNRAS, 404, 475
Johansen, A., Youdin, A., & Mac Low, M. 2009, ApJ, 704, L75
Johns-Krull, C. M., Valenti, J. A., & Koresko, C. 1999, ApJ, 516, 900
Jørgensen, J. K., van Dishoeck, E. F., Visser, R., et al. 2009, A&A, 507, 861
Kalas, P., Graham, J. R., Chiang, E., et al. 2008, Science, 322, 1345
Kant, I. 1755, Allgemeine Naturgeschichte und Theorie des Himmels, ed. Kant, I.
Kawabe, R., Ishiguro, M., Omodaka, T., Kitamura, Y., & Miyama, S. M. 1993, ApJ, 404, L63
Keene, J. & Masson, C. R. 1990, ApJ, 355, 635
Kenyon, S. J., Dobrzycka, D., & Hartmann, L. 1994, AJ, 108, 1872
Kessler-Silacci, J., Augereau, J., Dullemond, C. P., et al. 2006, ApJ, 639, 275
Koerner, D. W., Sargent, A. I., & Beckwith, S. V. W. 1993, Icarus, 106, 2
Krumholz, M. R., Cunningham, A. J., Klein, R. I., & McKee, C. F. 2010, ApJ, 713, 1120
Krumholz, M. R., McKee, C. F., & Klein, R. I. 2005, Nature, 438, 332
Kurz, R. & Shaver, P. 1999, The Messenger, 96, 7
Lacy, J. H., Knacke, R., Geballe, T. R., & Tokunaga, A. T. 1994, ApJ, 428, L69
Lada, C. J., Muench, A. A., Luhman, K. L., et al. 2006, AJ, 131, 1574
Lada, C. J. & Wilking, B. A. 1984, ApJ, 287, 610
Lagrange, A., Bonnefoy, M., Chauvin, G., et al. 2010, Science, 329, 57
Lahuis, F., van Dishoeck, E. F., Blake, G. A., et al. 2007, ApJ, 665, 492
Langkowski, D., Teiser, J., & Blum, J. 2008, ApJ, 675, 764
Laplace, P. S. 1796, Le Systeme du Monde, Vol. II, ed. Laplace, P. S.
Larson, R. B. 1969, MNRAS, 145, 271
Larson, R. B. 2003, Reports on Progress in Physics, 66, 1651
Léger, A., Rouan, D., Schneider, J., et al. 2009, A&A, 506, 287
Leinert, C., Zinnecker, H., Weitzel, N., et al. 1993, A&A, 278, 129
Lepp, S. & Dalgarno, A. 1996, A&A, 306, L21
Lommen, D., Jørgensen, J. K., van Dishoeck, E. F., & Crapsi, A. 2008, A&A, 481, 141
Lommen, D., Maddison, S. T., Wright, C. M., et al. 2009, A&A, 495, 869
Lommen, D. J. P., van Dishoeck, E. F., Wright, C. M., et al. 2010, A&A, 515, A77+
Love, S. G. & Pettit, D. R. 2004, in Lunar and Planetary Institute Conference Abstracts, Vol. 35, Lunar and Planetary Institute Conference Abstracts, ed. S. Mackwell & E. Stansbery, 1119
Luhman, K. L., Allen, P. R., Espaillat, C., Hartmann, L., & Calvet, N. 2010, ApJS, 186, 111
Mamajek, E. E. 2008, Astronomische Nachrichten, 329, 10
Marcy, G. W. & Butler, R. P. 1996, ApJ, 464, L147+
Marois, C., Macintosh, B., Barman, T., et al. 2008, Science, 322, 1348
Massi, M., Forbrich, J., Menten, K. M., et al. 2006, A&A, 453, 959
Massi, M., Menten, K., & Neidhöfer, J. 2002, A&A, 382, 152
Massi, M., Ros, E., Menten, K. M., et al. 2008, A&A, 480, 489
Mathieu, R. D., Stassun, K., Basri, G., et al. 1997, AJ, 113, 1841
Mayor, M. & Queloz, D. 1995, Nature, 378, 355
Merín, B., Brown, J. M., Oliveira, I., et al. 2010, ApJ, 718, 1200
Muzerolle, J., Calvet, N., Briceño, C., Hartmann, L., & Hillenbrand, L. 2000, ApJ, 535, L47
Narayanan, D., Kulesa, C. A., Boss, A., & Walker, C. K. 2006, ApJ, 647, 1426
Natta, A. 2008, Physica Scripta Volume T, 130, 014014
Natta, A., Testi, L., Calvet, N., et al. 2007, Protostars and Planets V, 767
Öberg, K. I., Qi, C., Fogel, J. K. J., et al. 2010, ArXiv e-prints

O'dell, C. R., Wen, Z., & Hu, X. 1993, ApJ, 410, 696
Panić, O. & Hogerheijde, M. R. 2009, A&A, 508, 707
Panić, O., Hogerheijde, M. R., Wilner, D., & Qi, C. 2008, A&A, 491, 219
Panić, O., Hogerheijde, M. R., Wilner, D., & Qi, C. 2009, A&A, 501, 269
Pascucci, I. & Tachibana, S. 2010, The Clearing of Protoplanetary Disks and of the Protosolar Nebula, ed. Apai, D. A. & Lauretta, D. S., 263–298
Paszun, D. & Dominik, C. 2009, A&A, 507, 1023
Patience, J., White, R. J., Ghez, A. M., et al. 2002, ApJ, 581, 654
Phillips, R. B., Lonsdale, C. J., & Feigelson, E. D. 1991, ApJ, 382, 261
Pollack, J. B., Hubickyj, O., Bodenheimer, P., et al. 1996, Icarus, 124, 62
Poppe, T., Blum, J., & Henning, T. 2000, ApJ, 533, 454
Qi, C. 2001, PhD thesis, CALIFORNIA INSTITUTE OF TECHNOLOGY
Queloz, D., Mayor, M., Weber, L., et al. 2000, A&A, 354, 99
Raghavan, D., Henry, T. J., Mason, B. D., et al. 2006, ApJ, 646, 523
Ricci, L., Testi, L., Natta, A., & Brooks, K. J. 2010a, ArXiv e-prints
Ricci, L., Testi, L., Natta, A., et al. 2010b, A&A, 512, A15+
Robitaille, T. P., Whitney, B. A., Indebetouw, R., Wood, K., & Denzmore, P. 2006, ApJS, 167, 256
Rodmann, J., Henning, T., Chandler, C. J., Mundy, L. G., & Wilner, D. J. 2006, A&A, 446, 211
Safronov, V. S. & Zvjagina, E. V. 1969, Icarus, 10, 109
Salter, D. M., Heißelmann, D., Chaparro, G., et al. 2009, Review of Scientific Instruments, 80, 074501
Salter, D. M., Hogerheijde, M. R., & Blake, G. A. 2008, A&A, 492, L21
Salter, D. M., Kóspál, Á., Getman, K. V., et al. 2010, ArXiv e-prints
Santos, N. C., Israelian, G., & Mayor, M. 2001, A&A, 373, 1019
Santos, N. C., Israelian, G., Mayor, M., Rebolo, R., & Udry, S. 2003, A&A, 398, 363
Sargent, A. I. & Beckwith, S. 1987, ApJ, 323, 294
Sargent, A. I. & Beckwith, S. V. W. 1991, ApJ, 382, L31
Schäfer, C., Speith, R., & Kley, W. 2007, A&A, 470, 733
Shu, F., Najita, J., Ostriker, E., et al. 1994, ApJ, 429, 781
Shu, F. H. 1977, ApJ, 214, 488
Sicilia-Aguilar, A., Hartmann, L., Calvet, N., et al. 2006, ApJ, 638, 897
Simon, M. & Guilloteau, S. 1992, ApJ, 397, L47
Simon, M. & Prato, L. 1995, ApJ, 450, 824
Skrutskie, M. F., Dutkevitch, D., Strom, S. E., et al. 1990, AJ, 99, 1187
Smith, B. A. & Terrile, R. J. 1984, Science, 226, 1421
Stahler, S. W. 1983, ApJ, 274, 822
Stassun, K. G., van den Berg, M., Feigelson, E., & Flaccomio, E. 2006, ApJ, 649, 914
Sterzik, M. F., Pascucci, I., Apai, D., van der Bliek, N., & Dullemond, C. P. 2004, A&A, 427, 245
Strom, K. M., Strom, S. E., Edwards, S., Cabrit, S., & Skrutskie, M. F. 1989, AJ, 97, 1451
Swedenborg, E. 1734, Opera Philosophica et Mineralia, ed. Swedenborg, E.
Tanaka, H., Himeno, Y., & Ida, S. 2005, ApJ, 625, 414
Taylor, G. B., Carilli, C. L., & Perley, R. A., eds. 1999, Astronomical Society of the Pacific Conference Series, Vol. 180, Synthesis Imaging in Radio Astronomy II
Terebey, S., Shu, F. H., & Cassen, P. 1984, ApJ, 286, 529
Terzieva, R. & Herbst, E. 1998, ApJ, 501, 207
Testi, L., Natta, A., Shepherd, D. S., & Wilner, D. J. 2001, ApJ, 554, 1087
Testi, L., Natta, A., Shepherd, D. S., & Wilner, D. J. 2003, A&A, 403, 323
Thi, W., Mathews, G., Ménard, F., et al. 2010, A&A, 518, L125+
Thi, W. F., van Dishoeck, E. F., Blake, G. A., et al. 2001, ApJ, 561, 1074

Udalski, A., Paczynski, B., Zebrun, K., et al. 2002, Acta Astron., 52, 1
Udalski, A., Szymanski, M., Kaluzny, J., Kubiak, M., & Mateo, M. 1992, Acta Astron., 42, 253
Udry, S. & Santos, N. C. 2007, ARA&A, 45, 397
van Kempen, T. A., van Dishoeck, E. F., Brinch, C., & Hogerheijde, M. R. 2007, A&A, 461, 983
van Zadelhoff, G., Aikawa, Y., Hogerheijde, M. R., & van Dishoeck, E. F. 2003, A&A, 397, 789
van Zadelhoff, G., van Dishoeck, E. F., Thi, W., & Blake, G. A. 2001, A&A, 377, 566
Visser, R. & Dullemond, C. P. 2010, ArXiv e-prints
Visser, R., van Dishoeck, E. F., Doty, S. D., & Dullemond, C. P. 2009, A&A, 495, 881
Walter, F. M. 1987, PASP, 99, 31
Weidenschilling, S. J. & Cuzzi, J. N. 1993, in Protostars and Planets III, ed. E. H. Levy & J. I. Lunine, 1031–1060
Weintraub, D. A., Zuckerman, B., & Masson, C. R. 1989, ApJ, 344, 915
Wilner, D. J., D'Alessio, P., Calvet, N., Claussen, M. J., & Hartmann, L. 2005, ApJ, 626, L109
Wilner, D. J., Ho, P. T. P., Kastner, J. H., & Rodríguez, L. F. 2000, ApJ, 534, L101
Wolf, S. & D'Angelo, G. 2005, ApJ, 619, 1114
Wolk, S. J. & Walter, F. M. 1996, AJ, 111, 2066
Yasui, C., Kobayashi, N., Tokunaga, A. T., Saito, M., & Tokoku, C. 2009, ApJ, 705, 54
Yorke, H. W., Bodenheimer, P., & Laughlin, G. 1993, ApJ, 411, 274